
Article:
Matthews, Edward and Dessent, Caroline E.H. orcid.org/0000-0003-4944-0413 (2018) Observation of Near-Threshold Resonances in the Flavin Chromophore Anions Alloxazine and Lumichrome. JOURNAL OF PHYSICAL CHEMISTRY LETTERS. pp. 6124-6130. ISSN 1948-7185

https://doi.org/10.1021/acs.jpclett.8b02529

Author Pre-acceptance manuscript

Observation of Near-Threshold Resonances in the Flavin Chromophore Anions Alloxazine and Lumichrome

Edward Matthews and Caroline E. H. Dessent*

Department of Chemistry, University of York, Heslington, York, YO10 5DD, UK.

* Corresponding Author: E-mail: caroline.dessent@york.ac.uk

ABSTRACT

Lumichrome (LC) is the chromophore of the flavin family of photoactive biomolecules, where key biochemical activity involves interplay between redox and photophysical events. Questions remain about the relationship between the redox status of the ground and excited states, and demand an improved understanding of the intrinsic photochemistry. Using anion photodissociation spectroscopy, we have measured the intrinsic electronic spectroscopy (564-220 nm) and accompanying photodegradation pathways of the deprotonated anionic form of LC. Experiments were also performed on alloxazine (AL), which is equivalent to LC minus two methyl groups. We observe a resonance state close to 3.8 eV for both anions for the first time, which we tentatively assign to dipole-bound excited states. For AL this state is sufficiently long-lived to facilitate dissociative electron attachment. Our results suggest that the presence of methyl group rotors at key positions along the molecular dipole may reduce the lifetime of the resonance state and hence provide a structural barrier to valence electron capture, and ensuing molecular dissociation.

GRAPHICAL ABSTRACT

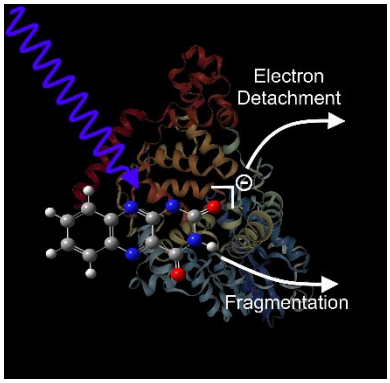

Flavin cofactors such as flavin mononucleotide (FMN) and flavin adenine dinucleotide (FAD) are amongst the most important photoactive biological molecules.[1] Despite the fact that there have been numerous investigations of the photochemistry and photophysics that underpin flavin photobiology,[2] critical questions remain about the sequence of light and redox events that occur, as well as the role of the protein around the central chromophore.[2-4] One approach to better understanding the photophysical properties of biomolecules is to study the chromophore as an isolated system in the gas-phase, an approach that has been productively applied to the green fluorescent protein chromophore.[5-7] Despite the importance of flavins, studies of the electronic properties of isolated (i.e. gas-phase) flavins have been extremely sparse until very recently,[8-10] particularly compared to the large number of studies where the chromophore is studied in solution.[11-13] This is surprising as the gas-phase is an appropriate medium in which to study intrinsic properties of such chromophores,[14] which typically sit entirely within a protein, since the vacuum dielectric constant ($\varepsilon_{vacuum} = 1$) is more similar to the immediate environment of the interior of a protein ($\varepsilon_{protein} = 2\text{-}4$) than for bulk water ($\varepsilon_{water} = 80$).[15]

Here, we present the first gas-phase study of the anionic (i.e. deprotonated) form of the smallest flavin chromophore lumichrome (LC), along with the simpler, related chromophore, alloxazine (AL). The structures of LC and AL are shown in Scheme 1. Our motivation for studying alloxazine is that it is often the subject of theoretical studies due to its modestly simpler structure that lacks the two aromatic methyl groups,[16,17] and the work we perform here allows us to investigate the extent to which these methyl groups affect the intrinsic electronic properties. Lumichrome is related to the biologically important FMN and FAD by loss of the ribose chain plus phosphate group, and the ribose chain plus adenosine diphosphate, respectively.

In choosing to focus on the simplest flavin chromophore, we deliberately adopt "bottom up" approach, where we begin by probing the properties of the simplest flavin chromophore, and will then sequentially reintroduce the molecular complexity in future experiments to build towards obtaining a complete understanding of intrinsic flavin chromophore electronic spectroscopy. We employ the general approach of forming the flavin chromophore anions as gas-phase species via electrospray of suitable solutions, and then obtaining the electronic spectrum via laser photodissociation spectroscopy.[18] Indeed, it is essential to begin a wider study of flavin chromophores by studying the smallest chromophore first, as larger flavin chromophores are known to fragment into smaller flavin chromophores following electronic excitation,[9,19] which offers the potential to seriously hamper spectral interpretation of the larger biological flavins. A complete knowledge of the properties of the smallest chromophore, will provide a firmer basis for both acquiring and interpreting experimental data for the larger systems.

The gaseous ion photodepletion and photofragment spectra of deprotonated AL and LC, i.e. $[AL\text{-}H]^-$ and $[LC\text{-}H]^-$, were recorded *in vacuo* using action spectroscopy in a laser-interfaced mass spectrometer which is described in detail elsewhere and in the Supporting Information (SI).[20,21] The photodepletion spectrum can be considered to be equivalent to the gaseous absorption spectrum, in the limit where excited state fluorescence is negligible.[22] Computational calculations (DFT and TDDFT) were performed on $[AL\text{-}H]^-$ and $[LC\text{-}H]^-$ using Gaussian 09 to determine the lowest-energy deprotonation isomers, dipole moments, electron detachment energies, and excitation spectra.[23] TDDFT has been used successfully in a number of recent experiments for interpreting the electronic spectra of similar anions, including in the

above threshold region e.g. for the luciferin anion,[24,25] supporting their use here to provide a preliminary interpretation of the spectra. The SI again includes further details.

Prior to acquiring the gaseous absorption spectra of $[AL-H]^-$ and $[LC-H]^-$, we obtained the aqueous alkaline (pH 10) absorption spectra of AL and LC (Figure S1). The absorption profiles are similar for the two systems, with both showing a region of relatively low absorption in the visible region between 500-300 nm, and a dominant UV band which peaks close to 260 nm, followed by the onset of a further band towards the high-energy spectral edge. Similar spectra have been published previously,[12,13,26]

Electrospray ionization readily produces $[AL-H]^-$ and $[LC-H]^-$ as gas-phase ions, with m/z 213 and 241, respectively. (Section S2 of the SI.) Figure 1a displays the photodepletion spectrum of $[AL-H]^-$. Four absorption bands (labelled **I** – **IV**) are evident, with the absorption onset occurring around 2.3 eV (540 nm). Band **I** is a relatively weak, broad band and is observed in the visible region, centred around 2.8 eV (443 nm). This band decreases in intensity above 2.8 eV and approaches a baseline level by 3.7 eV. An extremely sharp-onset band (**II**) is observed above 3.8 eV with a maximum at 4.05 eV (306 nm). Band **III** appears as another strong feature between 4.3-5.2 eV with a peak occurring at 4.81 eV (260 nm), while the rising edge of band **IV** is observed above 5.6 eV. An equivalent set of transitions are observed in the photodepletion spectrum of gaseous $[LC-H]^-$ (Figure 1b), with the λ_{max} of bands **I** – **IV** appearing at 2.6, 4.03, 4.74, and >5.6 eV respectively.

Comparing the solution and gaseous absorption spectra, both spectra display relatively low-intensity absorptions across the visible range, and it seems clear that the dominant UV solution-phase band, is related to the strong **III** feature in the gaseous spectrum. However, it is striking

that there is no solution-phase band close to 4.0 eV, the location of the sharp-onset feature, **II**, in the gaseous spectra. The very sharp onsets of the **II** features reveals that resonances are present for [AL-H] and [LC-H] at these energies, the first observation of such a feature for flavins. We discuss the assignment of the absorption spectra and the nature of this resonance further below.

We next turn to exploring the photofragment ions that are associated with the excited states evident in the Figure 1 spectra. Photofragmentation of $[AL-H]^-$ following excitation at 4.77 eV (260 nm – **III**) produces m/z 170 as the dominant ionic fragment which corresponds to the loss of 43 mass units (HNCO) from $[AL-H]^-$ (Section S4). HNCO has been identified as a uracil photofragment in several previous experiments.[27,28] A second, very minor fragment with m/z 142 is evident (at <1% intensity), corresponding to loss of HNCO and CO from the parent ion:

$$[AL-H]^- + h\nu \rightarrow \text{m/z 170} + \text{HNCO} \quad [1a]$$

$$\rightarrow \text{m/z 142} + \text{HNCO} + \text{CO} \quad [1b]$$

Similarly, when $[LC-H]^-$ is photoexcited at 4.77 eV, the major photofragmentation channels corresponding to loss of 43 and 71 mass units to produce photofragments with m/z 198 and 170, respectively:

$$[LC-H]^- + h\nu \rightarrow \text{m/z 198} + \text{HNCO} \quad [2a]$$

$$\rightarrow \text{m/z 170} + \text{HNCO} + \text{CO} \quad [2b]$$

These photofragments appear with similar intensities to the corresponding photofragments of $[AL-H]^-$. A number of minor photofragments with m/z 168, 169, 172, 482 and 483 are also observed. We note that the 482 and 483 photofragments appear to be heavier than the starting ion (m/z 241), but the 482 fragment is straightforwardly explained by the m/z 241 being comprised of both the $[LC-H]^-$ singly-charged monomer, and also the $([LC-H]^-)^2$ doubly-

charged dimer. Due to limitations in our ion isolation width, we also select m/z 241.5 in our starting ion package, which includes the +1 isotope peak of $([LC\text{-}H]^-)^2$ with a mass of 483 and a double negative charge. This is discussed more thoroughly in Section S5 of the SI, with the action spectrum for the m/z 482 photofragment being presented in Section S9 of the SI. It is important to stress that all of the m/z 168, 169, 172, 482 and 483 photofragments are very minor. Therefore, the fact that a single, strong photofragment ion is predominantly produced by $[AL\text{-}H]^-$ and $[LC\text{-}H]^-$ suggests that a single isomeric species of $[AL\text{-}H]^-$ and $[LC\text{-}H]^-$ is present in each the electrosprayed ion sample. This contrasts with other systems we have studied where multiple isomers are present.[29,30] Low-energy collision induced dissociation (CID) of $[AL\text{-}H]^-$ and $[LC\text{-}H]^-$ results in fragmentation with loss of HNCO, i.e. thermal excitation versions of Equations [1a] and [2a], hence mirroring the photofragmentation results where loss of HNCO is the major channel (Section S6).

Photofragment intensities are monitored in our experiment at each scanned wavelength to provide further insight into the nature of the excited states.[29,30] The action spectrum for production of the major photofragment from $[AL\text{-}H]^-$ with m/z 170 is displayed in Figure 2a, showing that the fragment is produced across the entire spectral range, with peaks in production within the regions of the band maxima **I** – **IV** of the photodepletion spectrum of $[AL\text{-}H]^-$ (Figure 1a). However, band **I** appears relatively more strongly in the photofragment action spectrum, whereas production of the fragment is notably flat across bands **II**-**IV** when compared to the photodepletion spectrum. The very sharp onset of photofragment production at ~3.8 eV, the onset of band **II** mirrors the photodepletion profile in this region.

Figure 2b shows the production spectrum of the dominant m/z 198 photofragment from $[LC\text{-}H]^-$. This spectrum is somewhat similar to the absorption spectrum of this species (Figure 1b)

but strikingly, production of m/z 198 does not peak across the region of band **II**. In particular, the sharp onset in spectral intensity seen in the absorption spectrum at ~3.8 eV, is completely absent from the photofragment action spectrum, indicating that the absorption process occurring in band **II** of $[LC-H]^-$ does not result in production of m/z 198. For anionic systems, any photodepletion that is not associated with photofragment production must be associated with electron loss processes.

DFT and TDDFT calculations were performed to allow us to provide a first interpretation of the experimental spectra, with a number of deprotonated species being identified (Section S7). Two relatively low-energy isomers were identified for both anions, which we label **1a** and **1b** for $[AL-H]^-$, and **2a** and **2b** for $[LC-H]^-$. Structures, relative energies and selected physical properties are given in Table 1. As the relative energies of the other deprotomeric isomers (SI) are substantially higher, we are confident that they are not present in this experiment. Deprotonation at position N1 (**1a** and **2a**) of the alloxazine ring is calculated to be more stable than deprotonation at position N3 (**1b** and **2b**) by 21.7 and 21.2 kJ mol^{-1} for AL and LC respectively. The vertical detachment energies (VDEs) of structures **1a** and **2a** are predicted to be 4.00 and 3.83 eV (310 and 324 nm) respectively, with the corresponding VDEs of structures **1b** and **2b** being significantly higher (4.64 and 4.71 eV respectively). Both **a** and **b** structures are highly polar, with dipole moments oriented primarily across the long axis of the molecule, indicating that the negative charge largely resides within the fused uracil ring section of the pteridine.

Figure 3 presents the TDDFT excitation spectra of structures **1a** and **1b** of $[AL-H]^-$ and **2a** and **2b** of $[LC-H]^-$, while the individual transitions that contribute to these spectra are included in the Supporting Information (Section S8). Comparing the calculated and experimental (Figure

1) spectra, it is evident that the calculated spectra of isomers **1a** and **2a** agree extremely well with the experimental spectra of $[AL-H]^-$ and $[LC-H]^-$, in terms of the agreement between the positions of bands **I** and **III**. Since the **a** isomers are calculated to be the lowest-energy isomers, this leads to a straightforward assignment of the gas-phase spectra as being associated with the **a** structure deprotomers. This situation is expected for a system where a single isomer has a significantly lower relative energy than the next highest isomer, both in solution and the gas-phase, and electrospray occurs in a protic solvent.[29,30] Inspection of the calculated spectra shows that there are no prominent electronic transitions in the **II** spectral region for either $[AL-H]^-$ and $[LC-H]^-$. However, the calculated VDEs (arrows on Figure 3) appear very close to the **II** experimental onsets.

We now return to considering the differences between the electronic spectra of $[AL-H]^-$ and $[LC-H]^-$, and the nature of feature **II** resonances. Having calculated the **1a/2a** VDEs for $[AL-H]^-$ to $[LC-H]^-$, as 4.00 and 3.83 eV, respectively, it is now clear that the sharp onsets of the band **II** resonance features correspond to the electron detachment thresholds of the anions. This leads us to tentatively assign the **II** features, as dipole-bound excited states.[31-34] We have found clear evidence for the formation of such states using our laser-interfaced mass spectrometry instrument following near-threshold excitation of anionic alkali halide salt clusters,[35] and are therefore confident that these states can be observed using our experimental approach. While dipole-bound states are prominent features of the electronic spectra of some anionic species, these transitions frequently become lower intensity on going from the gas-phase to solution,[34,36] consistent with the absence of a strong **II** feature in the solution-phase spectra. Since the negative ion resonances of LC/AL are currently entirely unknown, further theoretical studies are now warranted to further characterise assign the features observed here.

In support of our assignment of the near-threshold resonances as dipole-bound states, we note that the $[AL\text{-}H]^-$ photodepletion feature **II** displays a typical "peaked" profile of a dipole-bound excited state.[34] In contrast, the $[LC\text{-}H]^-$, band **II** displays a flatter top, a profile that has been associated with lower-magnitude dipoles (*i.e.* dipoles that are too small to critically bind an electron to form a stable dipole-bound state).[34] The shapes of the band **II** features therefore suggest that the vertical dipole moment for $[LC\text{-}H]^-$, is lower than that for $[AL\text{-}H]^-$. However, our calculations (Table 1) indicate that the vertical dipole moment of $[LC\text{-}H]^-$ is in fact modestly larger than that of $[AL\text{-}H]^-$, and both have similar orientations (Figure 4), so further factors must be at play.

One of the most intriguing results to emerge from our experiments is the observation that electron capture into the near-threshold resonance for alloxazine results in ionic fragmentation of $[AL\text{-}H]^-$ with production of the m/z 170 fragment along with neutral HNCO. This is evident in the way in which the production profile of the m/z 170 fragment matches the photodepletion profile of feature **II**. For lumichrome, electron occupation of this resonance state does not lead to molecular dissociation on a timescale that can compete with electron autodetachment. Thus, it is more correct to modify equations [1a] and [2a] for the **II** region to acknowledge the role of the transient negative ion (TNI) at the resonance;

$$[AL\text{-}H]^- + h\nu \rightarrow [AL\text{-}H]^{*-}\ (TNI) \rightarrow m/z\ 170 + HNCO \qquad [1c]$$

$$[LC\text{-}H]^- + h\nu \rightarrow [LC\text{-}H]^{*-}\ (TNI) \rightarrow e^-_{autodetach} + [LC\text{-}H] \qquad [2c]$$

In the **I** and **III** regions, in contrast, HNCO must be produced through rapid excited state decay followed by thermal dissociation on the electronic ground state surface. This leads to production of the m/z 170 and m/z 198 fragments as in collision induced dissociation (Section S6).[21]

Recent work from Neumark and co-workers using time-resolved anion photoelectron spectroscopy has provided a number of examples of dipole-bound states which can either autodetach or evolve into a valence anion, which subsequently dissociates. [37,38] Thus it is now well acknowledged that the formation of a dipole-bound state can act as a doorway to valence-anion formation, and hence to molecular dissociation.[37-40] This leads us to interpret that our spectroscopic observations as being consistent with $[AL-H]^-$ forming an above-critical threshold dipole-bound state in the region of the VDE, while $[LC-H]^-$ forms a sub-critical dipole-bound state. The dipole-bound state for $[AL-H]^-$ then acts as a doorway state to a valence state which leads to dissociation with loss of a neutral HNCO unit [1c]. In contrast, the sub-critical dipole moment of $[LC-H]^-$ is not stable on a timescale necessary for valence anion formation and results only in electron detachment [2c].

It is useful to reflect that the only structural difference between alloxazine and lumichrome, is the presence of lumichrome's two methyl groups. Brauman and co-workers investigated the effects of molecular rotation on the observation of dipole-bound states of anions via photodetachment studies of enolate anions in an ion cyclotron spectrometer over two decades ago.[41] In this seminal work, it was concluded that the binding of the electron by a dipole is very sensitive to the motions of the dipole. Of particular relevance to the current work were their results for pinacolone enolate, which was found to lack resonances associated with a dipole-bound state, due largely to the presence of internal rotors. From their studies of the series of enolates, they concluded that any molecular rotations can lead to shortening of the lifetime of the dipole-bound state. If the molecule has internal rotors, the internal and external rotations can couple, thus perturbing the angular momentum of the dipole, so that for molecules such as pinacolone enolate, the dipole-bound state will be very short lived. These

experimentally-driven interpretations were supported by a number of subsequent theoretical studies.[42-45]

The deprotonated $[LC-H]^-$ versus $[AL-H]^-$ systems studied here appear to present a striking example of the effect of methyl rotors on the stability of a dipole-bound excited state for a medium sized biologically relevant anion. Rotational constants and moments of inertia are included on Figure 4. What is evident from the orientation of the vertical dipole moments pictured in Figure 4 is that the methyl rotors will lie directly within the area of a dipole-bound state orbital.[31] As the lifetime of the dipole-bound excited state of $[LC-H]^-$ is shortened due to the presence of the internal rotors, there appears to be insufficient time for the dipole-bound state to evolve into a valence state which subsequently dissociates, compared to the timescale for autodetachment.[37,38]

As discussed in the introductory paragraphs, LC is the key structural component of the flavin family of biomolecules. Their activity as photoreceptors is closely linked to their redox properties, where a coupled two electron/two proton capture by the LC moiety leads to the reduced form.[2] The results presented here are important in this context since they reveal the presence of transient negative ion resonances that appear close to 4.0 eV, and provide a route for electron capture into the flavin valence framework. Intriguingly, the presence of the methyl groups which are present in LC compared to AL, appear to act to prevent single electron capture by LC resulting in dipole-bound state mediated molecular dissociation. More generally, we have gained significant new insight into the role that can be played by methyl internal rotors in preventing single electron capture that results in molecular dissociation. Further complementary studies using advanced imaging and time resolved techniques are desirable for

the important group of flavin molecules, as well as advanced theoretical studies to provide a deeper insight into the nature of their electron-capture properties.

■ ASSOCIATED CONTENT

Supporting Information

Further discussion of experimental and computational methods, the solution-phase absorption spectra of AL and LC, details of the electrospray ionization mass spectroscopy of AL and LC, photofragments mass spectra (4.77 eV) of $[AL-H]^-$ and $[LC-H]^-$, collision induced dissociation of $[AL-H]^-$ and $[LC-H]^-$, calculated relative energies of the deprotonation isomers of AL and LC, calculated electronic excitations for the TDDFT calculations of $[AL-H]^-$ and [LC-H] and photofragment action spectrum of the m/z 462 photofragment from the $[LC-H]^-$ mass peak
This material is available free of charge via the Internet at http://pubs.acs.org.

■ AUTHOR INFORMATION

Corresponding Author

*E-mail: caroline.dessent@york.ac.uk. Fax: 44-1904-322516.

Notes

The authors declare no competing financial interest.

■ ACKNOWLEDGMENTS

Acknowledgment is made to the Donors of the American Chemical Society Petroleum Research Fund for support or partial support of this research, through the award of grant ACS PRF 56174-ND6. We thank the University of York and the Department of Chemistry at the University of York for provision of funds for the Horizon OPO laser system, and the York Advanced Computing Cluster (YARCC) for access to computational resources.

REFERENCES

(1) Editorial. The Light Fantastic. *Nat. Chem. Biol.* **2014**, *10*, 483.

(2) Antill, L. M.; Woodward, J. R. Flavin Adenine Dinucleotide Photochemistry is Magnetic Field Sensitive at Physiological pH. *J. Phys. Chem. Lett.* **2018**, *9*, 2691-2696.

(3) Zanetti-Polzi, L.; Aschi, M.; Amadei, A.; Daidone, I.; Alternative Electron-Transfer Channels Ensure Ultrafast Deactivation of Light-Induced Excited States in Riboflavin Binding Protein. *J. Phys. Chem. Lett.* **2017**, *8*, 3321-3327.

(4) Conrad, K. S.; Manahan, C. C.; Crane, B. R. Photochemistry of Flavoprotein Light Sensors. *Nat. Chem. Biol*. **2014**, *10*, 801-809.

(5) Mooney, C. R. S.; Horke, D. A.; Chatterley, A. S.; Simperler, A.; Fielding, H. H.; Verlet, J. R. R. Taking the Green Fluorescence Out of the Protein: Dynamics of the Isolated GFP Chromophore Anion. *Chem. Sci.* **2013**, *4*, 921-927.

(6) Forbes, M.W.; Jockusch, R. A. Deactivation Pathways of an Isolated Green Fluorescent Protein Model Chromophore Studied by Electronic Action Spectroscopy. *J. Am. Chem. Soc.* **2009**, *131*, 17038-17039.

(7) Acharya, A.; Bogdanov, A. M.; Grigorenko, B. L.; Bravaya, K. B.; Nemukhin A. V., Lukyanov, K. A.; Krylov, A. I. Photoinduced Chemistry in Fluorescent Proteins: Curse or Blessing? *Chem. Rev.* **2017**, *117*, 758-795.

(8) Stockett, M. H. Photo-Induced Proton-Coupled Electron Transfer and Dissociation of Isolated Flavin Adenine Dinucleotide Mono-Anions. *Phys. Chem. Chem. Phys*. **2017**, *19*, 25829-25833.

(9) Guyon, L.; Tabarin, T.; Thuillier, B.; Antoine, R.; Broyer, M.; Boutou, V.; Wolf, J.-P.; Dugourd, P. Femtosecond Pump-Probe Experiments on Trapped Flavin: Optical Control of Dissociation, *J. Chem. Phys.* **2008**, *128*, 075103.

(10) Sheldrick, A.; Müller, D.; Günther, A.; Nieto, P.; Dopfer, O. Optical Spectroscopy of Isolated Flavins: Photodissociation of Protonated Lumichrome. *Phys. Chem. Chem. Phys*. **2018**, *20*, 7407-7414.

(11) Heelis, P. F. The Photophysical and Photochemical Properties of Flavins (Isoalloxazines). *Chem. Soc. Rev.* **1982**, *11*, 15-39.

(12) Drossler, P.; Holzer, W.; Penzkofer, A.; Hegemann, P. pH Dependence of the Absorption and Emission Behaviour of Riboflavin in Aqueous Solution. *Chem. Phys.* **2002**, *282*, 429-439.

(13) Penzkofer, A. Absorption and Emission Spectroscopic Investigation of Alloxazine in Aqueous Solutions and Comparison with Lumichrome. *J. Photochem. Photobiol. A: Chem.* **2016**, *314*, 114-124 and references therein.

(14) Andersen, L. H.; Bochenkova, A. V. The Photophysics of Isolated Protein Chromophores. *J. Eur. Phys. D* **2009**, *51*, 5-14.

(15) Simonson, T.; Brooks, C. L. Charge Screening and the Dielectric Constant of Proteins: Insights from Molecular Dynamics. *J. Am. Chem. Soc.* **1996**, *118*, 8452-8458.

(16) Chang, X. P.; Xie, X. Y.; Lin, S. Y.; Cui, G. QM/MM Study on Mechanistic Photophysics of Alloxazine Chromophore in Aqueous Solution. *J. Phys. Chem. A* **2016**, *120*, 6129-6136.

(17) Salzmann, S.; Marian, C.M. The Photophysics of Alloxazine: A Quantum Chemical Investigation in Vacuum and Solution. *Photochem. Photobiol. Sci.* **2009**, *8*, 1655–1666.

(18) Antoine, R.; Dugourd, P. Visible and Ultraviolet Spectroscopy of Gas-Phase Protein Ions. *Phys. Chem. Chem. Phys.* **2011**, *113*, 16494-16509.

(19) Bellina, B.; Brown, J. M.; Ujma, J.; Murray, P.; Giles, K.; Morrise, M.; Compagnon, I.; Barran, P. E. UV Photodissociation of Trapped Ions Following Ion Mobility Separation in a QTOF Mass Spectrometer. *Analyst*, **2014**, *139*, 6348-6351.

(20). Matthews, E.; Sen, A.; Yoshikawa, N.; Bergstrom E.; Dessent, C. E. H. UV Laser Photoactivation of Hexachloroplatinate Bound to Individual Nucleobases in Vacuo as Molecular Level Probes of a Model Photopharmaceutical. *Phys. Chem. Chem. Phys*. **2016**, *18*, 15143-15152.

(21) Sen, A.; Luxford, T. F. M.; Yoshikawa, N.; Dessent, C. E. H. Solvent Evaporation Versus Proton Transfer in Nucleobase–$Pt(CN)_{4,6}^{2-}$ Dianion Clusters: A Collisional Excitation and Electronic Laser Photodissociation Spectroscopy Study. *Phys. Chem. Chem. Phys*. **2014**, *16*, 15490-15500.

(22) Wellman, S. M. J.; Jockusch, R. A. Moving in on the Action: An Experimental Comparison of Fluorescence Excitation and Photodissociation Action Spectroscopy. *J. Phys. Chem. A*, **2015**, *119*, 6333-6338.

(23) Frisch, M. J.; Trucks, G. W.; Schlegel, H. B.; Scuseria, G. E.; Robb, M. A.; Cheeseman, J. R.; Scalmani, G.; Barone, V.; Mennucci, B.; Petersson, G. A.; et al. *Gaussian 09,* Revision D.01; Gaussian, Inc., Wallingford, CT, 2009.

(24) Noguchi, Y.; Hiyama, M.; Akiyama, H.; Koga, N. First-Principles Investigation on Rydberg and Resonance Excitations: A Case Study of the Firefly Luciferin Anion. *J. Chem. Phys.* **2014**, *141*, 044309.

(25) Støchkel, K.; Milne, B. F.; Nielsen, S. B. Spectrum of the Firefly Luciferin Anion Isolated in Vacuo. *J. Phys. Chem. A*, **2011**, *115*, 2155-2159.

(26) Tyagi, A.; Penzkofer, A. Absorption and Emission Spectroscopic Charaterization of Lumichrome in Aqueous Solutions. *Photochem. Photobiol*, **2011**, *87*, 524-533.

(27) Zhou, C.; Matsika, S.; Kotor, M.; Weinold, T. C. Fragmentation Pathways in the Uracil Radical Cation. *J. Phys. Chem. A*, **2012**, *116*, 9217-9227.

(28) Barc, B.; Ryszka, M.; Spurrell, J.; Dampc, M.; Limão-Vieira, P.; Parajuli, R.; Mason, N. J.; Eden, S. Multi-Photon Ionization and Fragmentation of Uracil: Neutral Excited-State Ring Opening and Hydration Effects**.** *J. Chem. Phys.* **2013**, *139*, 244311.

(29) Matthews, E.; Dessent, C. E. H. Locating the Proton in Nicotinamide Protomers via Low-Resolution UV Action Spectroscopy of Electrosprayed Solutions. *J. Phys. Chem. A*, **2016**, *120*, 9209-9216.

(30) Matthews, E.; Dessent, C. E. H. Experiment and Theory Confirm that UV Laser Photodissociation Spectroscopy Can Distinguish Protomers Formed Via Electrospray. *Phys. Chem. Chem. Phys.* **2017**, *19*, 17434-17440.

(31) J. Simons, Theoretical Study of Negative Molecular Ions**.** *Annu. Rev. Phys. Chem.* **2011**, *62*, 107-128.

(32) Zimmerman, A. H.; Brauman, J. I. Resonances in Electron Photodetachment Cross Sections. *J. Chem. Phys.* **1977**, *66*, 5823-5824.

(33) Zhu, G. Z.; Huang, D. H.; Wang, L. S. Conformation-Selective Resonant Photoelectron Imaging from Dipole-Bound States of Cold 3-Hydroxyphenoxide. *J. Chem. Phys.* **2017**, *147*, 013910.

(34) Dessent, C. E. H.; Kim, J.; Johnson, M. A. Photochemistry of Halide Ion-Molecule Clusters: Dipole Bound Excited States and the Case for Asymmetric Solvation. *Acc. Chem. Res*. **1998**, *31*, 527-534.

(35) Harvey, A. J. A.; Yoshikawa, N.; Wang, J. G.; Dessent, C. E. H. Communication: Evidence for Dipole-Bound Excited States in Gas-Phase $I^{-}{\cdot}MI$ (M = Na, K, Cs) Anionic Salt Microclusters. *J. Chem. Phys.* **2015**, *143*, 101103.

(36) Serxner, D.; Dessent, C.E.H.; Johnson, M. A. Precursor of the I^{-}_{aq} Charge-Transfer-to-Solvent (CTTS) Band in $I^{-}{\cdot}(H_2O)_n$ Clusters. *J. Chem. Phys*. **1996**, *105*, 7231-7234.

(37) Yandell, M. A.; King, S. B.; Neumark, D. M. Decay Dynamics of Nascent Acetonitrile and Nitromethane Dipole-Bound Anions Produced by Intracluster Charge-Transfer. *J. Chem. Phys.* **2014**, *140*, 184317.

(38) Li, W. L.; Kunin, A.; Matthews, E.; Yoshikawa, N.; Dessent C. E. H.; Neumark, D. M. Photodissociation Dynamics of the Iodide-Uracil (I^{-}U) Complex. *J. Chem. Phys*. **2016**, *145*, 044319.

(39) Matthews, E.; Cercola, R.; Mensa-Bonsu, G.; Neumark D. M.; Dessent, C. E. H. Photoexcitation of Iodide Ion-Pyrimidine Clusters Above the Electron Detachment Threshold: Intracluster Electron Transfer Versus Nucleobase-Centred Excitations. *J. Chem. Phys*. **2018**, *148*, 084304.

(40) Dessent, C. E. H.; Kim, J.; Johnson, M. A. Spectroscopic Observation of Vibrational Feshbach Resonances in Near-Threshold Photoexcitation of $X^-{\cdot}CH_3NO_2$ (X^- = I^- and Br^-). *Faraday Discuss.* **2000**, *115*, 395-406.

(41) Brinkman, E. A.; Berger, S.; Marks, J.; Brauman, J. I. Molecular Rotation and the Observation of Dipole-Bound States of Anions. *J. Chem. Phys*., **1993**, *99*, 7586-7594.

(42) Walthall, D. A.; Karty, J. M. Brauman, J. I. Molecular Rotations and Dipole-Bound State Lifetimes. *J. Phys. Chem. A* **2005**, *109*, 8794-8799.

(43) Ard, S. G.; Compton, R. N.; Garrett, W. R. Rotational Auto-Detachment of Dipole-Bound Anions. *Chem. Phys. Lett*. **2016**, *650*, 154-158.

(44) Clary, D. C. Photodetachment of Electrons from Dipolar Anions. *J. Phys. Chem.* **1988**, *92*, 3173-3181.

(45) Simons, J. Modified Rotationally Adiabatic Model for Rotational Autoionization of Dipole-Bound Molecular Anions. *J. Phys. Chem.* **1989**, *91*, 6858-6865.

SCHEMES AND FIGURE CAPTIONS

Scheme 1: Schematic diagram of the structures of AL (**1**) and LC (**2**). Atom labels are included on AL.

Figure 1: Photodepletion spectra of a) $[AL\text{-}H]^-$ and b) $[LC\text{-}H]^-$, across the range 2.20 – 5.64 eV (564 – 220 nm). The solid red lines are 5-point adjacent averages of the data points.

Figure 2: Photofragment production spectra of a) the m/z 170 photofragment from $[AL\text{-}H]^-$ and b) the m/z 198 photofragment from $[LC\text{-}H]^-$, across the range 2.20 – 5.64 eV (564 – 220 nm). The solid red lines are 5-point adjacent averages of the data points. The break in the m/z 198 spectrum between 3.45-3.6 eV corresponds to a region where no fragment ion is produced.

Figure 3: Calculated TDDFT absorption spectra of the (a) N1 deprotonated (**1a**) and (b) N3 deprotonated (**1b**) structures of $[AL\text{-}H]^-$, and the (c) N1 deprotonated (**2a**) and (b) N3 deprotonated (**2b**) structures of $[LC\text{-}H]^-$. The arrows indicate the positions of the calculated VDEs (Table 1). Oscillator strengths for the excitations are listed in Section S8 of the SI.

Figure 4: Schematic diagram illustrating the vertical dipole moments of isomers **a** of $[AL\text{-}H]^-$ (top) and $[LC\text{-}H]^-$ (bottom) calculated at the PBE0/6-311+G(d,p) level. The calculated moments of inertia and rotational constants are also shown.

FIGURES AND SCHEMES

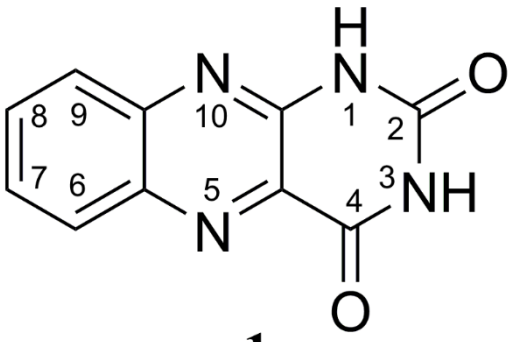

1

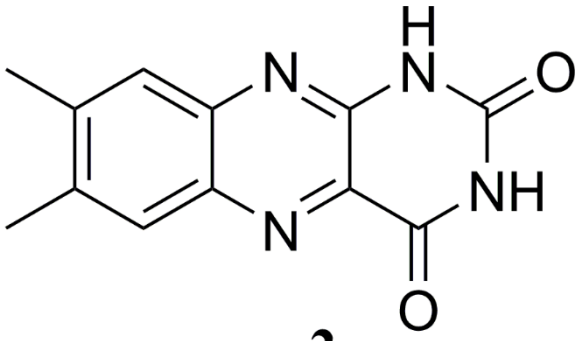

2

Scheme 1

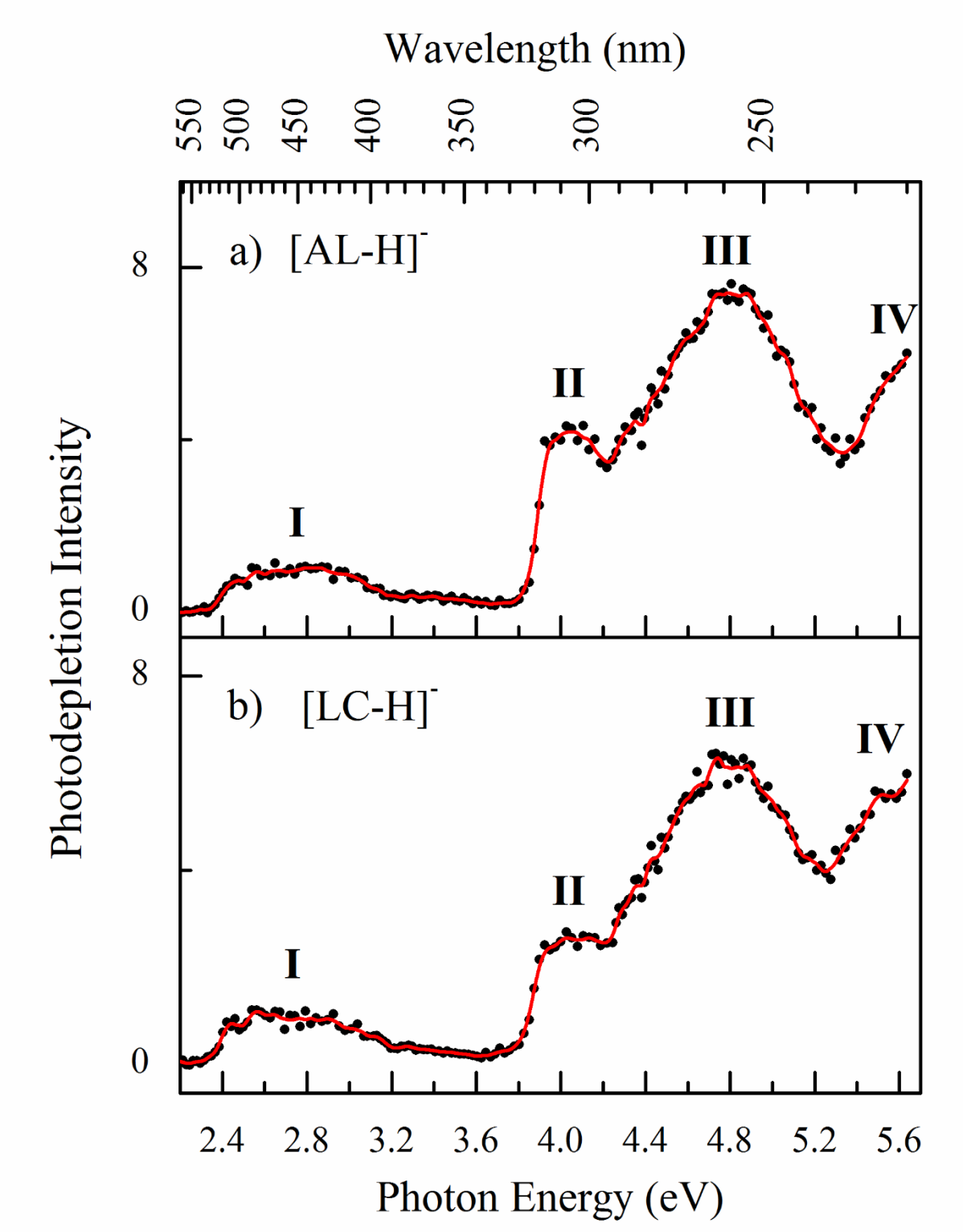
Wavelength (nm)
550
500
450
400
350
300
250
a) [AL-H]-
b) [LC-H]-
I
II
III
IV
8
0
Photodepletion Intensity
2.4
2.8
3.2
3.6
4.0
4.4
4.8
5.2
5.6
Photon Energy (eV)

Figure 1

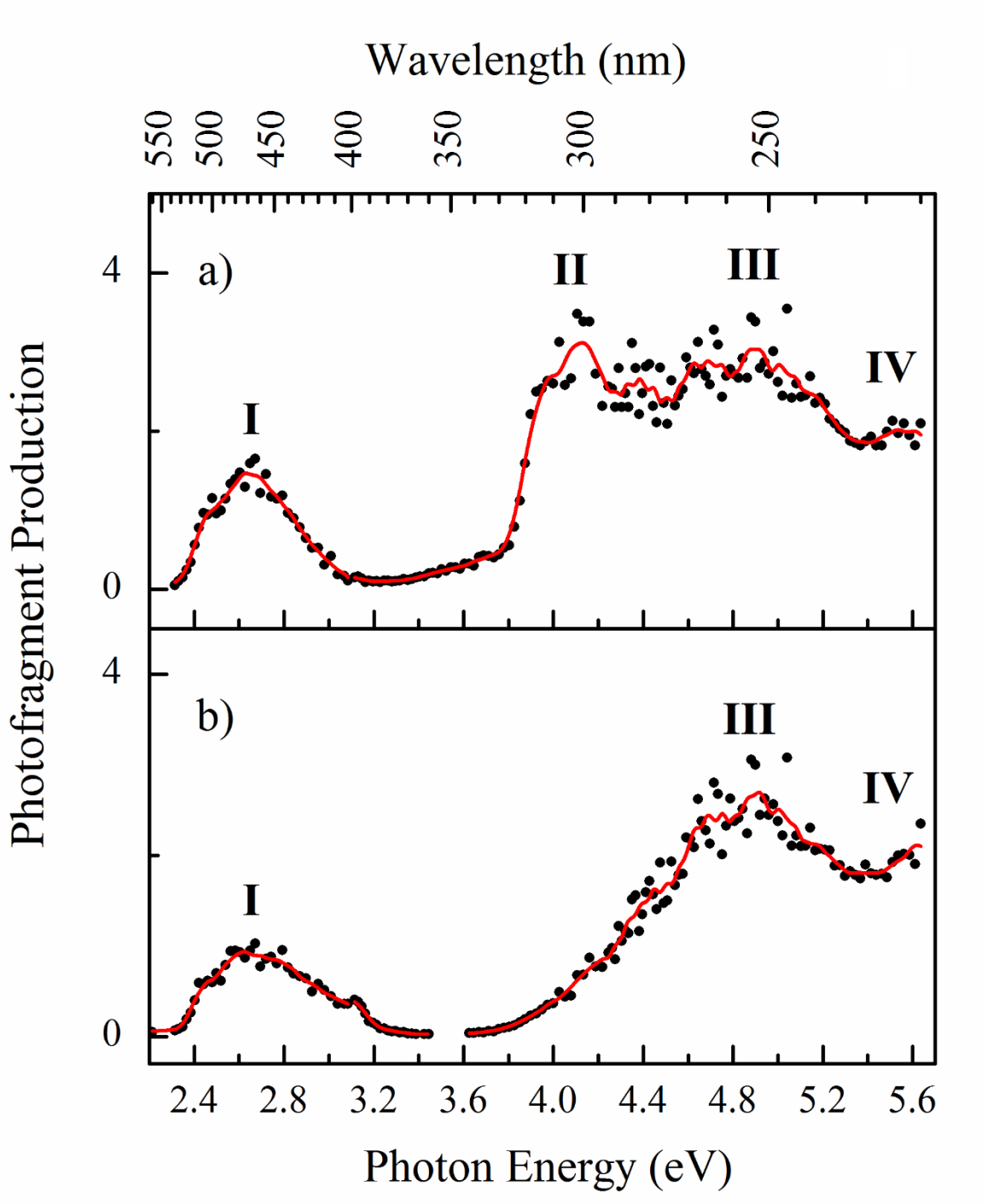
Wavelength (nm)
550
500
450
400
350
300
250
Photofragment Production
4
a)
II
III
IV
I
0
4
b)
III
IV
I
0
2.4
2.8
3.2
3.6
4.0
4.4
4.8
5.2
5.6
Photon Energy (eV)

Figure 2

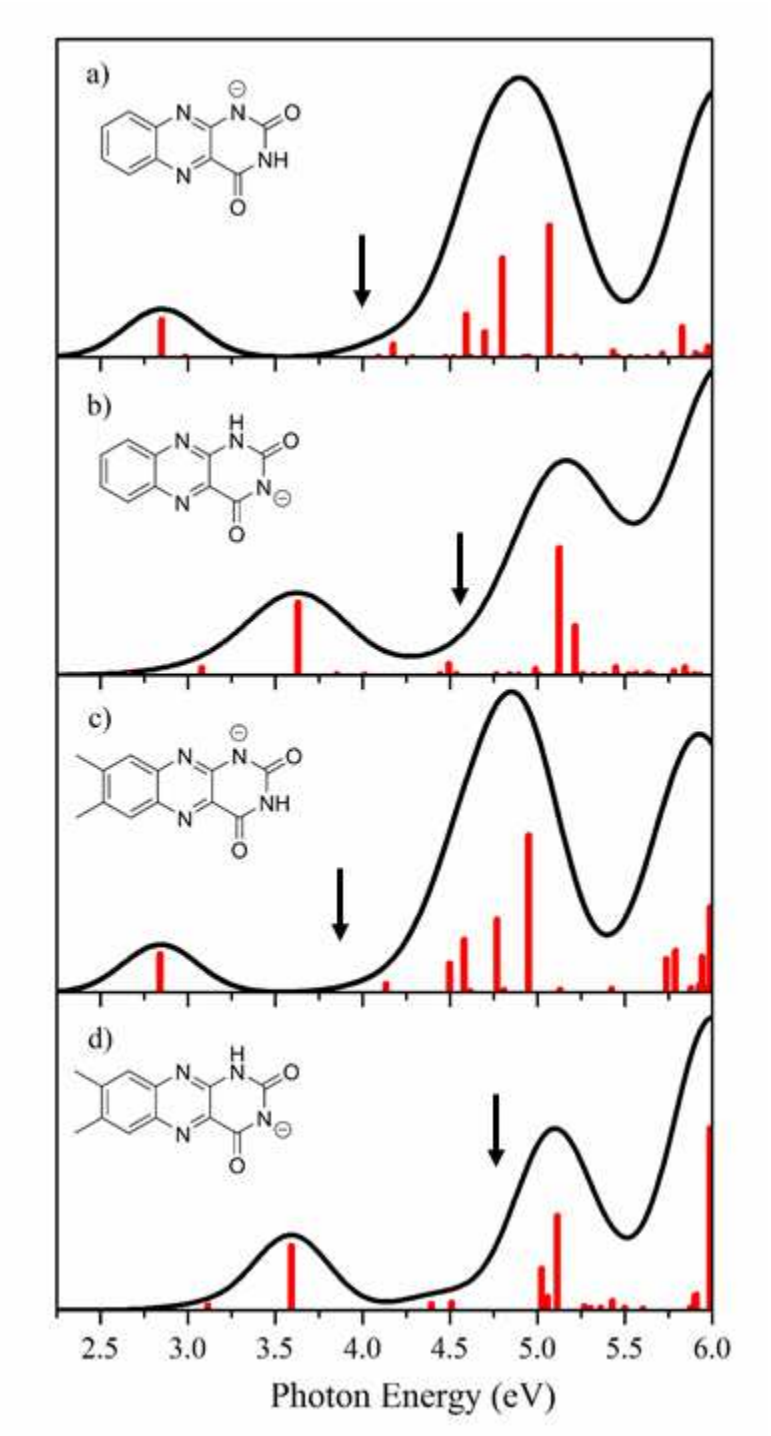

Figure 3

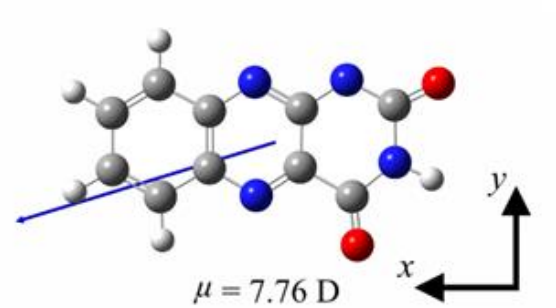

$\mu = 7.76$ D

$I_X = 1308.5$ a.u. $B_X = 1.379$ GHz
$I_Y = 5034.7$ a.u. $B_Y = 0.358$ GHz
$I_Z = 6343.2$ a.u. $B_Z = 0.285$ GHz

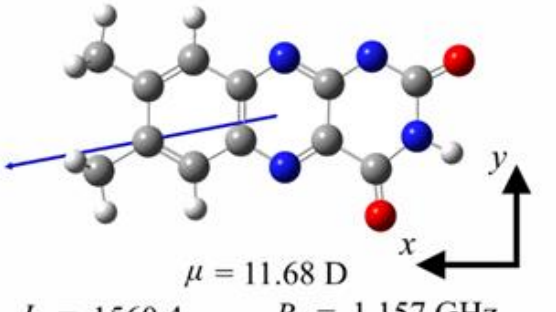

$\mu = 11.68$ D

$I_X = 1560.4$ a.u. $B_X = 1.157$ GHz
$I_Y = 7744.8$ a.u. $B_Y = 0.233$ GHz
$I_Z = 9283.0$ a.u. $B_Z = 0.194$ GHz

Figure 4

TABLES

Table 1: Calculated relative energies and physical properties of structures 1a, 1b, 2a and 2b of $[AL-H]^-$ and $[LC-H]^-$ calculated at the PBE0/6-311+G (d,p) level.[a,b] Relative electronic energies (ZPE corrected), vertical detachment energies, adiabatic detachment energies and dipole moments are shown.

Structure	Deprotonation Site	Relative Energy[b,c] (kJ mol^{-1})	VDE (eV)	ADE (eV)	Dipole Moment (D)	Vertical Dipole Moment[d] (D)
1a	N1	0.0 (0.0)	4.00	3.87	7.8	7.0
1b	N3	21.7 (6.01)	4.64	4.22	12.6	7.6
2a	N1	0.0 (0.0)	3.83	3.71	11.7	9.0
2b	N3	21.2 (5.25)	4.71	-	16.5	16.1

[a] See Figure 1 for definitions of the atom labels.
[b] The relative energies are zero-point energy corrected.
[c] Values in parentheses are calculated in water.
[d] The dipole moment of the vertical neutral molecule (*i.e.* neutral with the same geometry as the anion) formed when the excess electron is ionized from the anion.

GRAPHICAL ABSTRACT

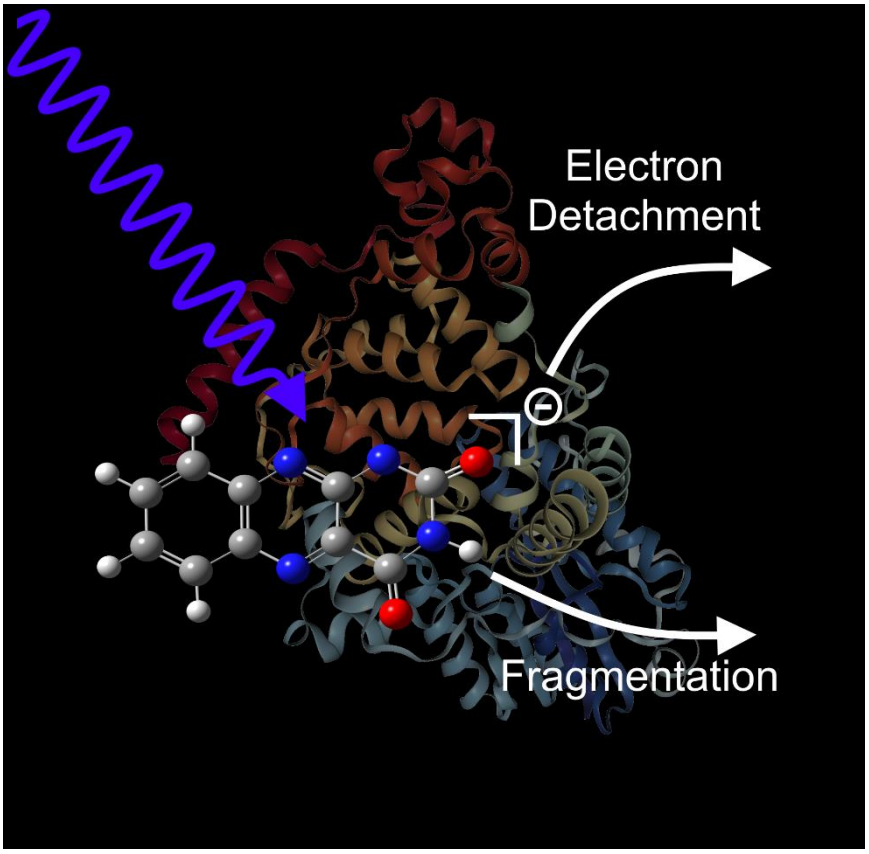

Supporting Information

Observation of Near-Threshold Resonances in the Flavin Chromophore Anions Alloxazine and Lumichrome

Edward Matthews and Caroline E. H. Dessent*

Department of Chemistry, University of York, Heslington, York, YO10 5DD, UK.

S1. Experimental and computational methods

The gaseous ion absorption and photofragment spectra of $[AL-H]^-$ and $[LC-H]^-$ were recorded *in vacuo* using action spectroscopy. UV-Vis photodissociation experiments were conducted in an AmaZon ion-trap mass spectrometer, which was modified for the laser experiments as described in detail elsewhere.[1,2] UV photons were produced by an Nd:YAG (10 Hz, Surelite) pumped OPO (Horizon) laser, giving ~1 mJ across the range 400 - 220 nm (3.10 – 5.64 eV) and ~0.5 mJ across the range 564 - 400 nm (2.20 – 3.10 eV). Scans were conducted using 1, 2 and 4 nm step sizes in the wavelength regions of 220 - 292, 292 - 400 and 400 - 564 nm respectively, the average energy difference between the data points is 0.02 eV. Photofragmentation experiments were run with an ion accumulation time between 20 – 100 ms with a fragmentation time of 100 ms, ensuring an average of one laser pulse per ion packet. The ion isolation width used was 0.7 m/z units, which provided the optimum balance of signal versus resolution for the systems studied. Total absorption is taken as the depletion in ion intensity of mass-selected ions, following irradiation, according to Equation 1:

$$\text{Photodepletion Intensity} = \text{Ln}\left(\frac{\text{Int}_{\text{OFF}}}{\text{Int}_{\text{ON}}}\right)/(\text{P} \times \lambda) \qquad \text{(Equation 1)}$$

Where Int_{ON} and Int_{OFF} are the intensities of the parent ion signals with and without irradiation respectively. Photodepletion is corrected for the number of photons by dividing the logarithmic depletion by the power of the tuneable laser (P) and the wavelength (λ). Power studies were conducted at several excitation wavelengths to determine the relationship between laser power and photodepletion, with the ~0.5 mJ power used being well within the region for single photon absorption. The photodepletion intensities of mass selected $[AL-H]^-$ and $[LC-H]^-$ ions have been averaged at each wavelength across the range 564 - 220 nm and are plotted against the energy of the excitation photons. The production of photofragments that are associated with the depletion of parent ions is calculated using equation 2, where Int_{Frag} is the ion intensity of each individual photofragment at a particular wavelength.

$$\text{Photofragmentation Production} = \left(\frac{\text{Int}_{\text{Frag}}}{\text{Int}_{\text{OFF}}}\right)/(\text{P} \times \lambda) \qquad \text{(Equation 2)}$$

A solution of AL and LC (1×10^{-5} mol L^{-1}) in methanol was introduced to the mass spectrometer through electrospray ionisation (ESI) using a nebulising gas pressure of 2.0 psi,

an injection rate of 300 μL/hr, a drying gas flow rate of 4.0 L min^{-1}, and a capillary temperature of 150ºC. Once electrosprayed, $[AL-H]^-$ and $[LC-H]^-$ (m/z 213 and 241 respectively) were mass isolated using the multiple reaction monitoring (MRM) functionality of the mass spectrometer. MRM enables different ions to be isolated and fragmented in sequential mass spectra. Using MRM, the mass spectra of four ions were obtained sequentially: $[AL-H]^-$ with irradiation, $[AL-H]^-$ without irradiation, $[LC-H]^-$ with irradiation and $[LC-H]^-$ without irradiation.

Multiple deprotonated structures of $[AL-H]^-$ and $[LC-H]^-$, were optimised using the PBE0/6-311+G(d,p) functional and basis set, using Gaussian 09. Frequency calculations were performed to ensure that all optimised structures correspond to true energy minima. All structures were also optimised using an implicit water solvent, with frequency calculations to show that the optimised structures were energy minima. Time-dependent density functional theory (TDDFT) calculations (30 states) were performed on the optimised gaseous structures of the two lowest energy structures of $[AL-H]^-$ and $[LC-H]^-$ (Figure 3 of the main text), at the PBE0/6-311+G(2d,2p) level.

References

1. E. Matthews, A. Sen, N. Yoshikawa, E. Bergstrom and C. E. H. Dessent, *Phys. Chem. Chem. Phys*. **18**, 15143 (2016).

2. A. Sen, T. F. M. Luxford, N. Yoshikawa, C. E. H. Dessent, *Phys. Chem. Chem. Phys*. ***16***, 15490-15500 (2014).

S2. Solution-phase absorption spectra of the deprotonation isomers of AL and LC

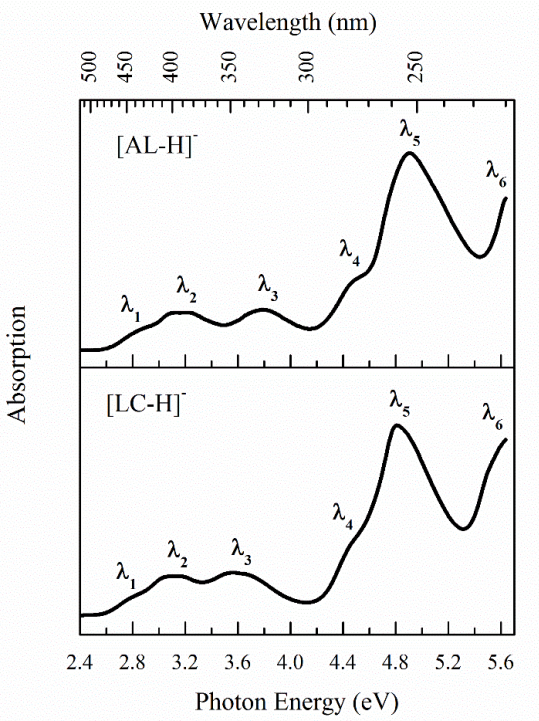

Figure S1: Aqueous absorption spectrum of a) $[AL-H]^-$ and b) $[LC-H]^-$ across the range 2.4 – 5.64 eV (517 – 220 nm). Bands are assigned in the table below.

Table S1: Assignment of features seen in the solution-phase absorption spectra of $[AL-H]^-$ and $[LC-H]^-$. The atom labels refer to Figure S2 below.

Transition	$[AL-H]^-$ Absorption Maximum / eV (nm)	$[LC-H]^-$ Absorption Maximum / eV (nm)	Isomer assignment
λ_1	2.80 (443) *sh*	2.76 (449) *sh*	**1b** (**2b**)
λ_2	3.17 (391)	3.11 (399)	**1a** (**2a**)
λ_3	3.78 (328)	3.56 (348)	**1a**, **1b** (**2a**, **2b**)
λ_4	4.46 (278) *sh*	4.45 (279) *sh*	**1b** (**2b**)
λ_5	4.90 (253)	4.81 (258)	**1a** (**2a**)
λ_6	>5.6	>5.6	

S3. Electrospray ionization mass spectroscopy of AL and LC

The electrospray ionization mass spectrum of a mixture of AL and LC, obtained in negative ion mode, is shown in Figure S2. The assignment of the prominent $[AL-H]^-$ and $[LC-H]^-$ deprotonated species is discussed in the main text. Here, we note that several intense contaminant peaks (m/z 255, 283, 297, 311, 325 and 339) are also evident. The m/z 255 and m/z 283 peaks are assigned as deprotonated palmitic and stearic acid,[19] which are known contaminants in mass spectrometry. The other peaks have mass differences of 14 m/z, indicating that these species are hydrocarbon contaminants which differ by a CH_2 group.

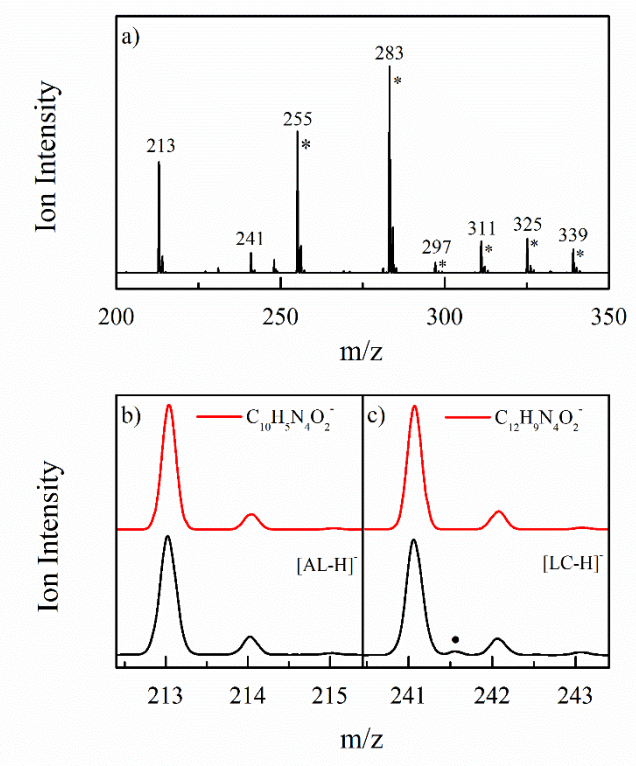

Figure S2: a) Total ion mass spectrum of an electrosprayed solution (MeOH) of AL and LC. Expanded spectra of the m/z region of b) $[AL-H]^-$ and c) $[LC-H]^-$ are included. The red lines are simulated isotope patterns for $[AL-H]^-$ ($C_{10}H_5N_4O_2^-$) and $[LC-H]^-$ ($C_{12}H_9N_4O_2^-$). * indicates a contaminant peak in the total ion spectrum. • indicates an ion with m/z 241.6.

S4. Photofragment mass spectrum of $[AL-H]^-$ photoexcited at 4.77 eV

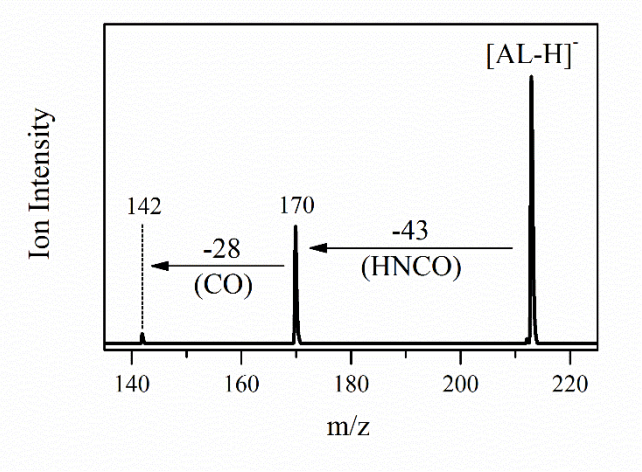

Figure S3: Photofragment mass spectra of $[AL-H]^-$ excited at 4.77 eV (260 nm). Neutral losses required to produce the photofragments are included.

S5. Photofragment mass spectrum of $[LC-H]^-$ photoexcited at 4.77 eV

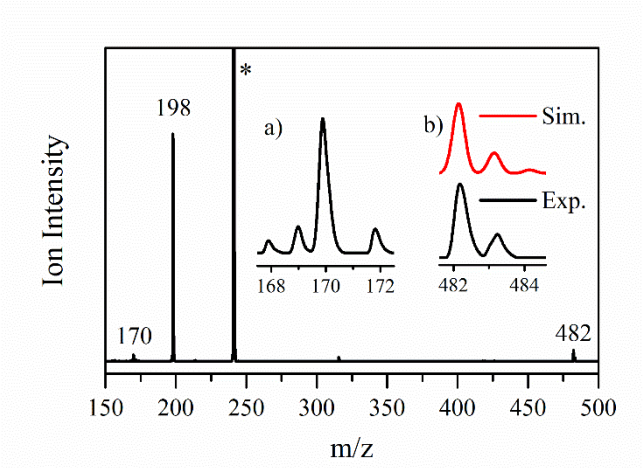

Figure S4: Photofragment mass spectra of $[LC-H]^-$ excited at 4.77 eV (260 nm). Insets show a zoomed mass spectrum between a) m/z 168 – 172 and b) m/z 482 – 484, the red line is a simulated isotope distribution pattern of $[LC-H]^{\bullet}$·$[LC-H]^-$ ($C_{24}H_{18}N_8O_4$).

Figure S4 displays the photofragment mass spectrum observed when of $[LC\text{-}H]^-$ excited at 4.77 eV. As discussed in the main text, the main photofragments observed when $[LC\text{-}H]^-$ is photoexcited at 4.77 eV correspond to loss of 43 and 71 mass units to produce photofragments with m/z 198 and 170, respectively. Additional weak photofragments with m/z 168, 169, 172, 482 and 483 are also observed, with the production of the m/z 482 and 483 photofragments being particularly striking since these photofragments appear to have masses greater than the mass of the starting ion. This is straightforwardly explained since the mass spectral values quoted here are m/z values, not simple masses. The observation of the m/z 482 photofragment is consistent with the presence of an $([LC\text{-}H]^-)_2$ doubly charged-dimer in the isolated m/z 214 ion packet that is unavoidably selected in the laser experiment. The $([LC\text{-}H]^-)_2$ species can lose an electron following photoexcitation to produce $[([LC\text{-}H])_2]^-$, which has m/z = 482 The m/z = 483 photofragment is produced in an entirely analogous manner, from the $([LC\text{-}H]^-)_2$ starting ion which has one unit of mass more than due to isotope contributions from C13 atoms. This is clearly demonstrated by the match of the experimental mass spectrum in Figure S4b, with the simulated isotope pattern. The m/z = 483 photofragment has been produced from a m/z = 241.5 starting ion, which has amu of 483 and a double negative charge. As noted in Section S1, the ion isolation width used in these experiments was 0.7 m/z units, so that photoexcitation has been conducted on m/z = 241 as well as m/z = 241.5, producing the m/z = 482 and m/z = 483 photofragments. Assignment of all photofragments is included in Table S2.

Table S2: Photofragments and assignments for [AL-H]- and [LC-H]-.

$[AL-H]^-$ Fragments		$[LC-H]^-$ Fragments	
m/z	Assignment	m/z	Assignment
170	$[AL-H-HNCO]^-$	198	$[LC-H-HNCO]^-$
142	$[AL-H-HNCO-CO]^-$	170	$[LC-H-HNCO-CO]^-$
		482	$[LC-H]\cdot[LC-H]^{\bullet-}$
		483[a]	$[LC-H]\cdot[LC-H]^{\bullet-}$
		168	$[LC-H-HNCO-C_2H_6]^-$
		169	$[LC-H-HNCO-C_2H_5]^{\bullet-}$
		172	$[LC-H-HNCO-C_2H_2]^-$

[a] The +1 mass isotope peak compound of the 482 species.

S6. Collision Induced Dissociation of deprotonated AL and LC

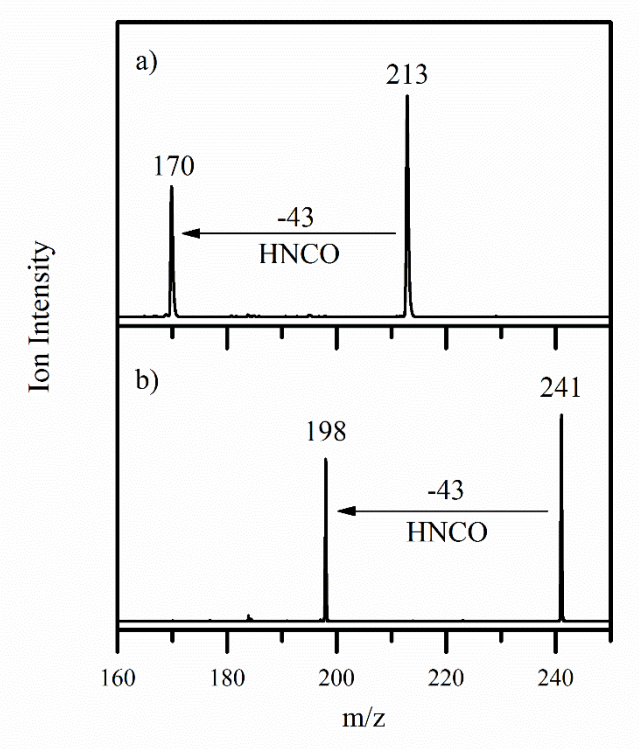

Figure S5: CID mass spectra of a) $[AL-H]^-$ and b) $[LC-H]^-$ fragmented with a fragmentation amplitude of 0.47 V for $[AL-H]^-$ and 0.43 V for $[LC-H]^-$. Neutral losses required to produce the photofragments are included.

S7. Calculated relative energies of the deprotonation isomers of AL and LC

Table S3: Relative energies (zero point energy corrected) of the deprotonation isomers of $[AL-H]^-$ and $[LC-H]^-$. The atom labels refer to Figure S6 below.

Structure	Protonated	$[AL-H]^-$ Rel. Energy / kJ mol^{-1}		$[LC-H]^-$ Rel. Energy / kJ mol^{-1}	
		Gaseous	Aqueous	Gaseous	Aqueous
a	N3	0.0	0.0	0.0	0.0
b	N1	21.7	6.01	21.2	5.25
c	CO2	52.0	45.5	51.9	45.1
d	CO4	76.9	64.6	77.0	64.1
e	N5	147.0	97.0	147.2	94.4
f	N10	115.2	60.6	115.6	59.9

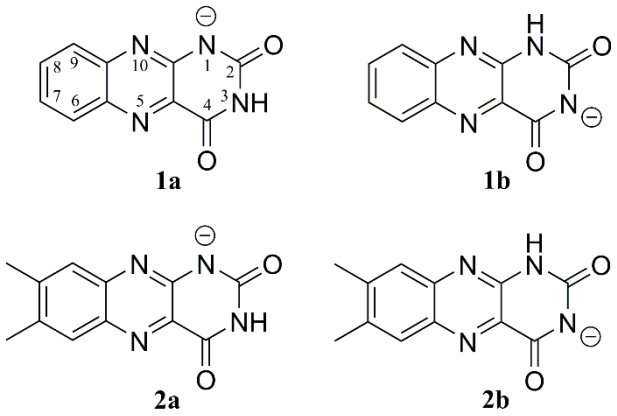

Figure S6: Schematic diagram to illustrate the lowest-energy isomers of deprotonated AL and LC. Atom labels used in Table S1 are included on structure 1a.

S8. Calculated Electronic Excitations for the TDDFT calculations of $[AL-H]^-$ and $[LC-H]^-$

Table S4: TDDFT Calculated Electronic Excitations and Oscillator Strengths (PBE0/6-311+G(2d,2p)) of Isomer 1a of $[AL-H]^-$

Transition Energy (eV)	Oscillator Strength
Alloxazine (**1a**) π → π* Transitions	
2.85	0.128
4.17	0.043
4.59	0.146
4.70	0.087
4.80	0.342
5.07	0.455
5.83	0.103
5.91	0.014
Alloxazine (**1a**) Lone Pair σ → σ* Transitions	
5.43	0.019
5.71	0.013
5.94	0.005
5.97	0.036

Table S5: TDDFT Calculated Electronic Excitations and Oscillator Strengths (PBE0/6-311+G(2d,2p)) of Isomer 1b of [AL-H]$^-$

Transition Energy (eV)	Oscillator Strength
Alloxazine (**1b**) π → π* Transitions	
3.08	0.021
3.63	0.226
4.49	0.018
5.13	0.398
5.22	0.153
5.45	0.023
Alloxazine (**1b**) Lone Pair σ → σ* Transitions	
5.11	0.006
5.78	0.011
5.84	0.023

Table S6: TDDFT Calculated Electronic Excitations and Oscillator Strengths (PBE0/6-311+G(2d,2p)) of Isomer 1a of $[LC-H]^-$

Transition Energy (eV)	Oscillator Strength
Lumichrome (**2a**) π → π* Transitions	
2.84	0.143
4.13	0.031
4.50	0.107
4.58	0.196
4.77	0.271
4.81	0.009
4.95	0.584
5.43	0.014
5.79	0.154
5.92	0.026
5.94	0.133
5.99	0.316
Lumichrome (**2a**) Lone Pair σ → σ* Transitions	
4.62	0.005
5.43	0.011
5.74	0.123
5.88	0.021
5.95	0.021
5.97	0.016

Table S7: TDDFT Calculated Electronic Excitations and Oscillator Strengths (PBE0/6-311+G(2d,2p)) of Isomer 1b of [LC-H]$^-$

Transition Energy (eV)	Oscillator Strength
Lumichrome (**2b**) π → π* Transitions	
3.11	0.020
3.59	0.262
4.39	0.024
4.51	0.031
5.02	0.169
5.11	0.386
5.27	0.016
5.30	0.009
5.43	0.037
5.90	0.059
5.91	0.062
5.99	0.743
Lumichrome (**2b**) Lone Pair σ → σ* Transitions	
5.06	0.051
5.36	0.010
5.50	0.010
5.60	0.007
5.87	0.010

S9. Photofragment action spectrum of the m/z 482 photofragment from the [LC-H]$^-$ mass peak

The photofragment production spectrum of m/z 482, produced from m/z 241, is shown in Figure S7. The identity of this fragment has been discussed in Section S5 and is likely to be a cluster of two [LC-H]$^-$ molecules with a single negative charge, originating from a dianionic dimer. The m/z 482 production spectrum shows that the threshold for ionising the dimer is ~3.7 eV. m/z 482 is produced as a trace fragment up to 4.2 eV, whereupon the production increases strongly as the photon energy increases. The production spectrum does not peak within band **III**, or indeed in bands **I** and **II**, of the [LC-H]$^-$ photodepletion spectrum (Figure 2b). This indicates that electron detachment from the dimer occurs by directly absorbing a photon with energy greater than the electron binding energy, rather than auto-detachment from an excited state or via multiphoton ionisation.

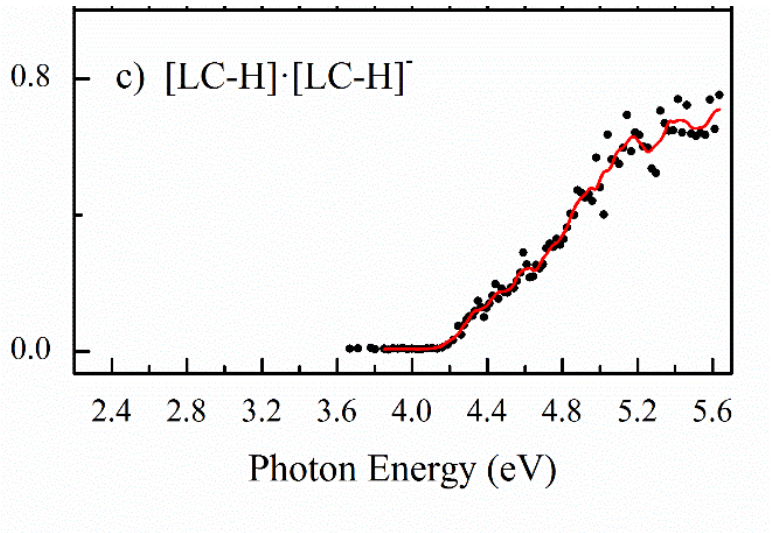

Figure S7: Photofragment action spectrum for [LC-H]·[LC-H]$^-$ (m/z = 482) produced from m/z = 241 parent ion.